Additive Manufacturing 55 (2022) 102857

Contents lists available at ScienceDirect

Additive Manufacturing

journal homepage: www.elsevier.com/locate/addma

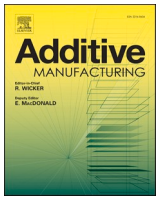

Research paper

# Novel backbone modified polyetheretherketone (PEEK) grades for powder bed fusion with enhanced elongation at break

Nan Yi [a,*], Richard Davies [a], Adam Chaplin [b], Oana Ghita [a]

[a] College of Engineering, Mathematics and Physical Sciences, University of Exeter, Exeter EX4 4QF, UK
[b] Victrex PLC, Hillhouse international, Thornton Cleveleys, Lancashire FY5 4QD, UK

ARTICLE INFO

*Keywords:*
Poly aryl ether ketone
Powder bed fusion
Crystallisation kinetics
Structure-property relationship

ABSTRACT

This study presents a new family of backbone modified polyetheretherketone (PEEK) grades in the powder bed fusion (PBF) process, coded as PAEK1 and PAEK2, with the same chemical structure but different molecular weights. By incorporating polyetherbiphenyletherketone (PEDEK) comonomer, the optimal powder bed temperature of the new grades could be reduced to 290 °C, approximately 40 °C lower than that of PEEK. The underlying crystallisation kinetics in the PBF process was investigated by replicating the in-process temperature profiles using a flash differential scanning calorimetry (DSC) machine. This method enabled monitoring of the development of crystallisation during the process and at different deposition thicknesses. The results confirmed that the PAEK2 grade with a higher molecular weight is slower crystallising. A significant part of the crystallisation of PAEK2 was found taking place in the later stage of the printing process, i.e. the free cooling stage. This leads to a better particle coalescence and enhanced elongation, a feature previously difficult to obtain in the PBF process. The PBF PAEK2 tensile bars achieved a significant increase in mechanical performance with an outstanding 13% in elongation, reaching its yielding point. The data supports that PAEK2 is the first high temperature polymer grade in the PBF process to match its bulk mechanical properties while maintaining a high level of crystallinity in the printed parts.

## 1. Introduction

Amongst the seven classes of additive manufacturing (AM) technologies, powder bed fusion (PBF) has the most potential to achieve large-scale production. Recently, the application of polyaryletherketones (PAEKs) in PBF is rapidly growing due to a need to combine the design freedom provide by PBF with the excellent properties of PAEKs, such as their high service temperatures, good mechanical properties, and compatibility with the high standards from industries such as aerospace sectors [1–3].

Polyetherketone (PEK) produced by EOS with the tradename of "EOS PEEK HP3" is the first and currently the only commercial neat high temperature polymer for PBF [4,5]. The optimal powder bed temperature of PEK HP3 has been identified to be 365 °C [6]. Adopting this high level of processing temperature brings challenges not only in maintaining these temperatures during printing, but also in recycling the unused powder after long build times. The high processing temperature induces severe thermo-oxidative degradation and cross-linking in used PEK powder [5]; hence the re-usage is not recommended by EOS [4]. Driven by economic factors such as the high cost of virgin PAEK powders and their low recyclability, novel grades tailored for PBF are desirable.

To meet the aforementioned challenges, the most direct way is to adopt existing commercial PAEK grades with lower melting temperatures than that of PEK in the high temperature PBF process. For PAEKs, their melting temperatures are known to be strongly dependent on their chemical structures, more specifically, their backbone compositions. As documented by Gardner et. al. [7], the melting temperatures of PAEK homopolymers are positively proportional to the ratio of ketone on their backbones, owing to the enhanced packing efficiency produced when increasing ketone linkages. Therefore, polyetheretherketone (PEEK) has been viewed as a potential candidate to replace PEK in the high temperature PBF process. Compared to PEK, the ketone concentration of PEEK drops from 50% to 33%, thereby suppressing the melting point by approximately 30 °C.

Attempts have been made to employ Victrex PEEK 450PF [8], and Victrex PEEK 150PF [9] in the high temperature PBF process, although they were originally developed for other manufacturing processes such as injection moulding or compression moulding [10]. The work of

* Corresponding author.
*E-mail address:* N.Yi@exeter.ac.uk (N. Yi).

https://doi.org/10.1016/j.addma.2022.102857
Received 16 December 2021; Received in revised form 20 March 2022; Accepted 25 April 2022
Available online 29 April 2022

Berretta et. al. [6] revealed that the optimal powder bed temperatures are 332 °C for PEEK 450PF, and 338 °C for PEEK 150PF, respectively, which are approximately 30 °C lower than that of PEK. However, one drawback of using PEEK in PBF is that the mean tensile strength of the printed PEEK 450PF tensile bars are 20 MPa lower than those made of PEK HP3 [8]. Another drawback is that, for PEEK 450PF, significant changes in crystallinity and melt rheology has been detected after ageing at 340 °C for 6 h [11], implying poor recyclability of PEEK 450PF after long building times.

An alternative approach is to develop new PAEK grades specifically for the high temperature PBF process. New PAEK grades with even lower melting temperatures could be synthesised by modifying the molecular backbone structure of PEEK, without sacrificing its high service temperature. Recently, Victrex has developed a copolymer based on PEEK, commercially launched for the fused filament fabrication (FFF) process [10]. By introducing polyetherbiphenyletherketone (PEDEK) co-monomers, the melting point could be tuned down to around 300 °C [12].

Inserting PEDEK units onto the molecular backbone of PEEK changes the crystallisation kinetics as well [13]. Remarkably slower crystallisation speed has been discovered under the influence of the PEDEK units [12]. As fast crystallisation hinders the interlayer diffusion, vertical FFF bars printed with slow crystallising PAEK copolymer present significant higher tensile strengths than those printed with neat PEEK [12]. In PBF, adhesion is also the key to better mechanical properties. Therefore, new PAEK grades that contain PEDEK units are promising candidates in the high temperature PBF process.

In printing semi-crystalline polymers, the mechanical properties of final parts are heavily influenced by the crystallisation processes. Investigating the isothermal crystallisation behaviour in respect to their PBF processing temperature windows is becoming a standard procedure for screening powders [14–18]. However, the isothermal assumption is found to be only valid for the few top layers during the building-step [19]. Throughout most of the processing time, powder is experiencing non-isothermal crystallisation. Hence, studies on crystallisation under a series of constant cooling rates have been conducted [15–17], hoping to provide information that is more relevant. Yet, the link between those experiments and the actual PBF process is weak for two reasons: (1) the cooling rates in the actual process are constantly changing [19] and (2) the range of cooling rates in PBF is difficult to monitor and has not been documented yet for the PBF process of high temperature polymers [20]. To advance our knowledge on crystallisation behaviour that better resembles the crystal growth in the PBF process, accurate in-process temperature profiles and methods to follow the crystallisation of powder under these temperature profiles are needed.

This paper presents two PAEK grades referred to as Victrex PAEK1 and Victrex PAEK2 in which PAEK2 has significant promise in the high temperature PBF process. A method to generate more accurate in-process temperature profiles is proposed. These profiles were constructed by combining analytical modelling results and in-situ measurements. Thermal analyses revealed the dynamic crystallisation kinetics at the selected powder bed depths of both grades during the PBF process. The key factors in achieving better mechanical property for PBF specimens were investigated.

## 2. Materials and experimental

### 2.1. Materials

Developmental grades Victrex PAEK1 and Victrex PAEK2 powders were provided by Victrex. The chemical structure and transition temperatures are disclosed in Section 3.1. Before printing, both powders went through a heat treatment (220 °C for 24 hr) to improve their flow properties. The treated powders present the average particle size D(50) of 58.61 μm for PAEK1 and 52.58 μm for PAEK2. The conditioned bulk densities for PAEK1 and PAEK2 are 0.38 g/cm$^3$ and 0.33 g/cm$^3$ measured by a Freemen FT-4 powder rheometer, respectively. The particle size and shape analysis were summarised in Figs. S-1 and S-2 in the Supplementary Material. No major differences were identified between PAEK1 and PAEK2.

### 2.2. Printing parameters

To compare the mechanical properties of the printed parts, ISO 527–2–1 A type tensile bars were printed in the XY plane using an EOS P800 system. Detailed schematic of the EOS P800 system has been provided in a previous study [20]. For printing both grades, the chamber temperature was set at 290 °C, whilst the building platform temperature at 260 °C. Laser power of 16.5 W was applied with a scan speed of 2550 mm/s and a hatching distance of 0.25 mm. After hatching, a post-sintering time of 12 s was imposed to stabilise the powder bed temperature. The layer thickness was set at 0.12 mm. The recoating speed was 200 mm/s. Prior to printing the tensile specimens, 10 mm thick powder bed was deposited to shield the thermal penetration from the building platform.

### 2.3. Processing temperature measurement

To acquire accurate in-process temperature profiles, in-situ measurements of the chamber temperature and the building platform temperature were carried out via the standard EOS P800 pyrometer. This integral setup enables the pyrometer to monitor the temperature of the uppermost layer. Temperature readings of the surface of the powder bed with five defined thicknesses (namely 3.2 mm, 5 mm, 8 mm, 11 mm, and 20 mm) during the control cooling stage and the free cooling stage were recorded as a function of the processing time. Categorisation of the building and cooling stages is provided in Section 3.2.1. The thermal conductivity of PAEK family is 0.32 W/m/K [10]. At this level, the thermal conductivity is barely sensitive to the effect of molecular weight [21]. For this reason, PAEK2 powder was used in all the measurements to construct the temperature profiles.

### 2.4. Thermal analysis

#### 2.4.1. Isothermal crystallisation

Protocols of using conventional differential scanning calorimetry (DSC) to track the isothermal crystallisation at the low and the high temperature regions and flash DSC for the medium temperature region have been established prior to this work [12]. In the current study, isothermal crystallisations at 170 – 190 °C (via the cold-crystallisation isothermal test protocol [12]) and 250 – 290 °C (via the isothermal from melt test protocol [12]) were measured by a Mettler Toledo DSC1. For each test, around 5 mg mass of PAEK1 or PAEK2 powder was packed in a standard Aluminium pan, encapsulated by a standard Aluminium lid. All conventional DSC tests were purged by a Nitrogen flow of 50 ml/min. Isothermal crystallisations at 200 – 240 °C (via the discontinuous isothermal test protocol [12]) were measured by a Mettler Toledo flash DSC2+ with UFS 1-type chip sensors. For each chip sensor, two PAEK1 or PAEK2 particles with the diameter of approximately 50 μm were placed onto the membrane via a brush pen hair, followed by a pre-melt heating ramp at 0.5 °C/s to 310 °C to fixate the particles. All flash DSC tests were purged by a Nitrogen flow of 80 ml/min.

#### 2.4.2. Dynamic in-process crystallisation

To investigate the in-process crystallisation, the constructed temperature profiles were simulated in the flash DSC. Initially a heating ramp from 30 °C to 370 °C at a rate of 1000 °C/s was imposed to remove the thermal history of the specimen. Next, the specimen was cooled down to 290 °C (i.e. the chamber temperature) at a rate of 1000 °C/s and held isothermally for 50 s to mimic the stabilisation step in the EOS P800 system. Then, to simulate the temperature profiles, multiple checkpoints were created along each profile and linear approximation was applied to

**Table 1**
Transition temperatures, ketone contents, and viscosities of PAEKs.

| Material | Transition temperatures (°C) | | | Ketone content (%) | Shear viscosity (Pa. s)[a] |
|---|---|---|---|---|---|
| | Tg | Tm | Tc | | |
| **EOS HP3** | 164 | 372 | 332 | 50% | 200 |
| **PEEK 450PF** | 143 | 339 | 297 | 33% | 350 |
| **PEEK 150PF** | 143 | 343 | 303 | 33% | 130 |
| **PAEK1** | 157 | 301 | 242 | 31% | 300 |
| **PAEK2** | 152 | 298 | 243 | 31% | 350 |

[a] According to ISO 11443, measured at 400 °C and a shear rate of 1000 $s^{-1}$.

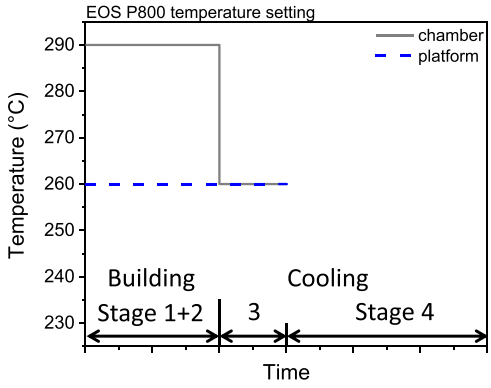


**Fig. 1.** Four stages of temperature setting in a complete print cycle using an EOS P800 system: Stage 1 – laser emission, Stage 2 – powder recoating, Stage 3 – controlled cooling, Stage 4 – free cooling.

connect any adjacent checkpoints, due to only constant heating or cooling rate can be executed in the flash DSC. At each checkpoint, the specimen was quenched to 30 °C at a cooling rate of 1000 °C/s to freeze the crystalline phase. Finally, a subsequent heating scan from 30 °C to 370 °C at a heating rate of 1000 °C/s was implemented to extract the endothermic melting peak in order to calculate the cumulative crystallinity at this checkpoint.

### 2.5. Crystallinity by X-ray diffraction

The overall crystallinities of the PBF and the injection moulded specimens were examined by wide angle X-ray diffraction (WAXD) measurements. In this paper, the intensity profile along the Bragg angle was obtained from a Bruker D8 Advance XRD diffractometer with Cu Kα radiation (λ = 0.154 nm). All measurements were performed in the "Locked Couple" mode with a 2θ range of 9–45°. The beam was generated at 40 kV and 40 mA. The diffraction profiles were obtained in a "Step Scan" method at a scan speed of 0.5 s/step. The degree of crystallinity can be calculated from the deconvoluted peaks:

$$X_C = \frac{\sum S_C}{S_A + \sum S_C} \quad (1)$$

where $S_A$ is the area of the amorphous peak, and $S_C$ is the area of the crystalline peak.

### 2.6. Mechanical tests

The mechanical properties of PAEK specimens were examined by uniaxial tensile tests using a Shimadzu standard tensile/compression machine equipped with a 20 kN load cell. Tensile moduli were assessed at a constant crosshead speed of 1 mm/min. Tensile strengths and values of elongation at break were evaluated at 5 mm/min. Ten repeats of each test condition were carried out under room temperature.

## 3. Results & discussions

### 3.1. New PAEK grades

PAEK1 and PAEK2 are two novel PAEK grades. Comparing to PEK and PEEK, both grades have lower melting temperatures ($T_m$), lower recrystallisation temperatures ($T_c$), but comparable glass transition temperatures ($T_g$), see Table 1. One possible reason for the differences in transition temperatures could be the lower concentration of ketone group on the molecular backbone of PAEK1 and PAEK2, which prompts a reduced chain mobility. Development of such PAEK grades holds great promise for PBF. It enables lower processing temperatures without comprising the relatively high service temperature of PAEK materials.

The only difference between PAEK1 and PAEK2 is the molecular weight. PAEK2 has a higher molecular weight which is similar to that of PEEK 450PF, signalled by the value of shear viscosity. It is well known that, for PEEK materials, higher molecular weight supresses crystallisation [22] and promotes larger elongation at break values of moulded specimens [23]. To what extent and how this impacts the application in the PBF process is the focus of the follow-on discussions.

### 3.2. Temperature profiles in the powder bed fusion process

#### 3.2.1. Temperature settings

Investigating crystallisation during PBF demands reliable temperature profiles over the whole process. The first step towards acquiring those profiles is to define the multiple stages of the process and outline the respective temperature settings. It is generally recognised that there are three successive phases in the PBF process, namely a pre-heating phase, a building phase, and a cooling phase. In this study, the pre-heating phase to make the EOS P800 system meet the temperature settings of the building phase was excluded in all flash DSC simulations, because the pre-heating phase is irrelevant to the investigation on crystallisation of PAEK powders. As illustrated in Fig. 1, the building phase is followed by the cooling phase, with each phase containing two stages.

The building phase comprises a laser emission stage (Stage 1) and a powder recoating stage (Stage 2) in succession, repeating as many times as the number of layers required to complete the parts. During the entire building phase, the chamber temperature was set at 290 °C whilst the building platform temperature was set at 260 °C. The succeeding cooling phase contains a controlled cooling stage (Stage 3) and a free cooling stage (Stage 4). Completion of the last layer commences the controlled cooling stage. At this stage, the chamber temperature was automatically switched to 260 °C by the system, matching the building platform temperature. Once the surface of the powder bed dropped to 260 °C, the heating was turned off altogether by the system, launching the free cooling stage until the powder bed reached room temperature and was ready for parts removal.

#### 3.2.2. In-process temperature profiles

In the current study, temperature profiles of two defined positions within the powder bed, namely $z_0 = 3.2$ mm and $z_{140} = 20$ mm, were constructed. Thickness $z_n$ is the distance from the building platform along the upright z-axis. The subscript $n$ marks the corresponding $n$-th layer at this thickness. As designed by the EOS P800 system, a minimum amount of powder deposition is mandatory to avoid the collision between the recoater and the building platform. Therefore, the minimum thickness of powder bed is $z_0$ of 3.2 mm.

Each in-process temperature profile consists of three segments, as displayed in Fig. 2. The first segment represents cooling of the $n$-th layer during powder deposition. The cooling is caused by the $n$-th layer incrementally moving downwards away from the heat source in the chamber. Moreover, the newly deposited layers act as a thermal insulator for the heat sources in the chamber. The cooling trends of this segment were generated by an analytical model, based on the

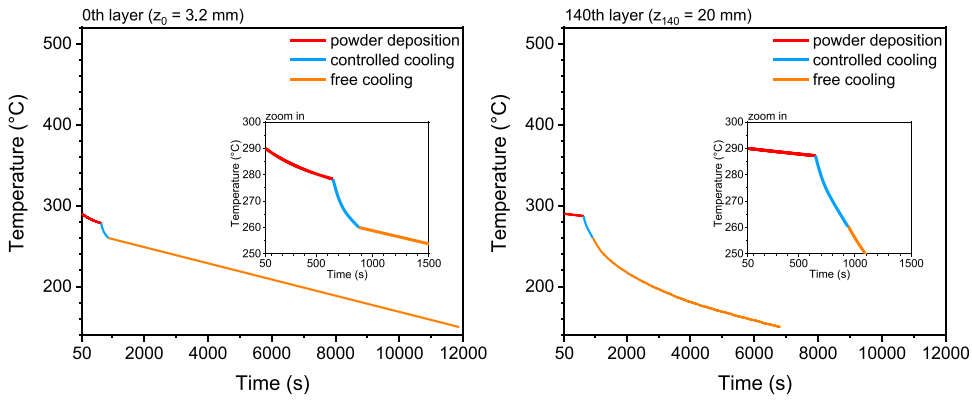


**Fig. 2.** In-process temperature profiles for the 0th layer ($z_0 = 3.2$ mm) and the 140th layer ($z_{140} = 20$ mm) excluding the laser emission. Construction method is described in Appendix.

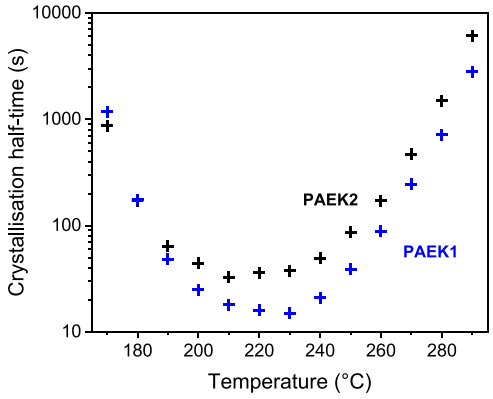


**Fig. 3.** Isothermal crystallisation kinetics of PAEK1 and PAEK2.

temperature settings of the building phase, along with other printing parameters listed in Section 2.2. This segment was modelled for 10 min to account for the deposition of approximately 2 mm thick powder above the *n*-th layer, matching the minimal thickness of a tensile bar according to ISO 527. Development of this model is described in the Appendix. The modelling results were found in reasonably good agreement with the measurements from literature on polyamides [19].

The second segment is the temperature drop during the controlled cooling stage. Profiles of this segment were obtained by monitoring the pyrometer readings at the surface of the powder bed with varied thicknesses under the temperature settings disclosed above. Overall, PAEK powder at $z_0 = 3.2$ mm exhibits slower cooling rates than powder at $z_{140} = 20$ mm, in line with the observations on PBF of polyamide powder [24].

The third and the final segment is the temperature drop when all heating elements were switched off. At $z_0 = 3.2$ mm, the temperature of powder is mainly influenced by the temperature of the building platform. Rapid temperature equalisation between powder at $z_0$ and the building platform is expected. For this reason, the cooling trend of powder at $z_0$ is considered following the same cooling trend of the building platform. In parallel, at $z_{140} = 20$ mm, the temperature of powder is heavily influenced by the temperature of the chamber. Similarly, the cooling trend of powder at $z_{140}$ is considered following the same cooling trend of the chamber. Recordings of the building platform temperature and the chamber temperature during the free cooling stage are shown in the Appendix.

The purpose of constructing these temperature profiles is to simulate them in the flash DSC to explore the crystallisation behaviour accordingly. The laser emission stage is not explicitly illustrated in Fig. 2 for two reasons. First, the temperature surge caused by laser emission

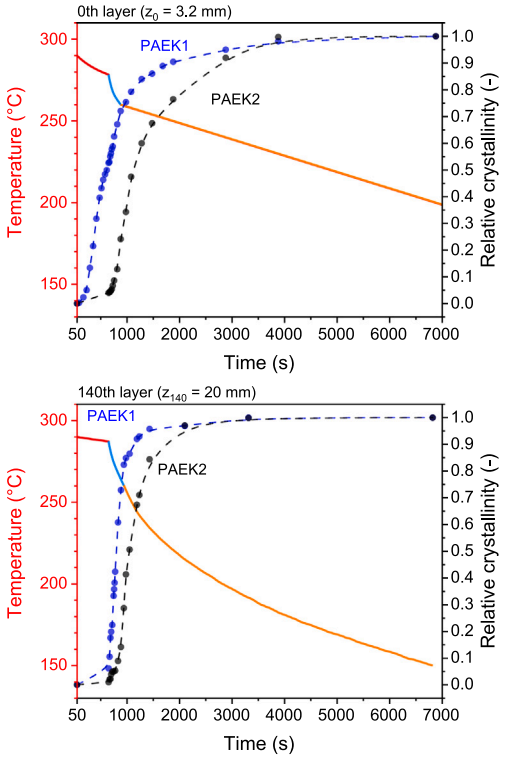


**Fig. 4.** Dynamic crystallisation kinetics of PAEK1 and PAEK2 while printing at the 0th layer ($z_0 = 3.2$ mm) and the 140th layer ($z_{140} = 20$ mm). Dash lines are trends.

stabilises back to the powder bed temperature within 0.1 s [25]. The short time scale makes it difficult to visualise. Second, the exact temperature profile of laser emission is still unknown [25]. For practical reasons, in the flash DSC, the laser emission was simulated by a fast heating ramp to 370 °C followed by a fast cooling ramp to 290 °C, as described in Section 2.4.2. The temperature was held isothermally for 50 s to mimic the stabilisation step after laser emission. Hence, in Fig. 2, the onset point of processing time is 50 s

### 3.3. Crystallisation kinetics

#### 3.3.1. Isothermal crystallisation

To quantify the crystallisation speeds of PAEK1 and PAEK2, their crystallisation half-times under isothermal conditions were documented in Fig. 3. It is evidenced that the higher molecular weight of PAEK2 leads

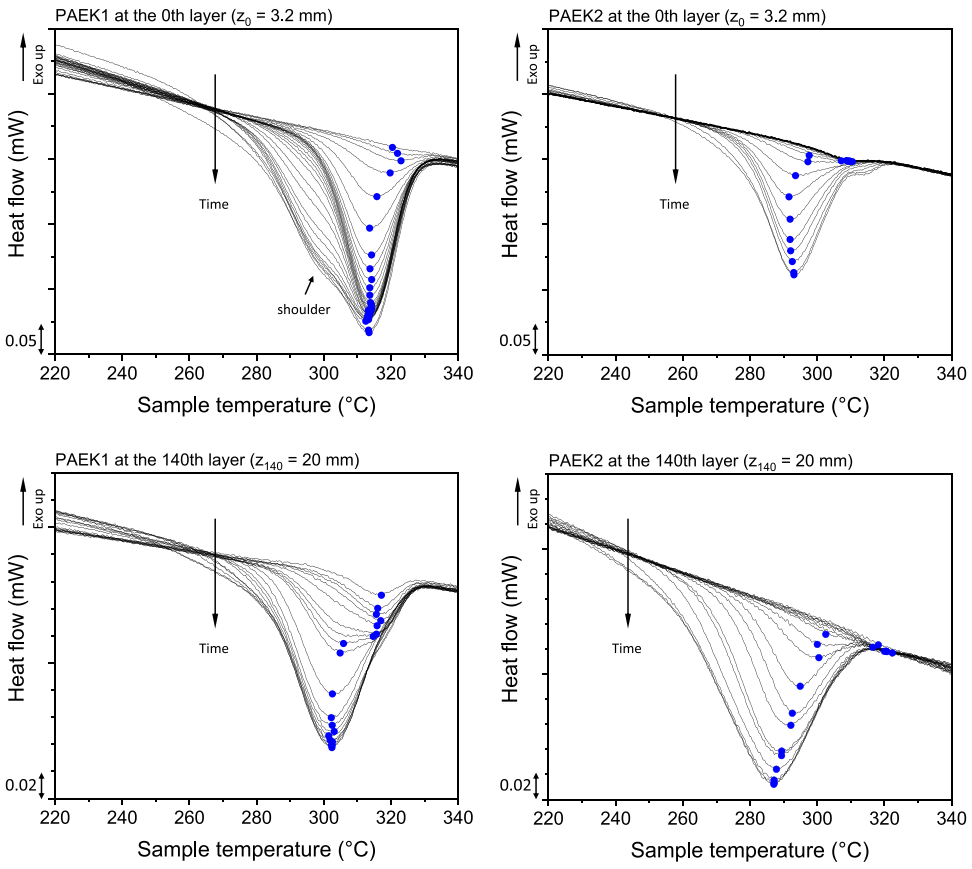


**Fig. 5.** Evolution of crystallisation following the simulated temperature profiles. The melting peak points were marked by the blue dots. The arrow with "Time" indicates the direction of time increase.

to significantly slower crystallisation speeds, due to the restricted chain mobility. At the powder bed temperature of 290 °C, the crystallisation half-time of PAEK2 is 6126 s while the half-time of PAEK1 is 2782 s. By contrast, PEEK450 has a half-time around 24 s at 290 °C, two decades faster than the half-times of the novel grades at the same temperature.

### 3.3.2. *Dynamic crystallisation during laser PBF*

The fast cooling rate of 1000 °C/s enforced by the flash DSC brings a unique opportunity to effectively map the crystal growth. Along the simulated temperature profiles, the specimen was quenched then remelted at each checkpoint to track the crystallisation behaviour under these changing cooling rates. The evolution of relative crystallinities for $z_0 = 3.2$ mm and $z_{140} = 20$ mm was plotted as a function of time in Fig. 4, respectively. It is evident that PAEK2 crystallises slower than PAEK1. At $z_0 = 3.2$ mm close to the building platform, PAEK1 completed more than half of its crystallisation (53%) at the end of powder deposition segment, whereas PAEK2 only initiated 4% of its crystallisation during this first segment. Regarding PAEK2 at $z_0$, the majority of crystallisation (87%) occurred at the final free cooling stage, whilst PAEK1 only developed 27% of the crystalline phase during the final stage.

At $z_{140} = 20$ mm farther away from the building platform, the temperature profile of the powder deposition segment is closer to a quasi-isothermal condition of 290 °C than at $z_0$. At the end of this first segment, PAEK1 reached 6% of relative crystallinity whereas PAEK2 barely crystallised with 1% of relative crystallinity. Again, PAEK2 at $z_{140}$ completed the majority of crystallisation (71%) at the final free cooling stage. By contrast, PAEK1 at $z_{140}$ developed most of its crystallisation (76%) during the controlled cooling stage. The crystallisation kinetics in Fig. 4 suggests that the farther away from the building platform, the less significant the difference in crystallisation behaviour between PAEK1 and PAEK2.

To further analyse the development of crystal morphology, the endothermic melting peaks of all the checkpoints were compiled in Fig. 5. It is noticeable in Fig. 5 that the melting points of PAEK1 are at a higher value than those of PAEK2. Moreover, the melting point shifts to lower temperatures with increasing processing time under all test conditions. Both phenomena could be explained by the fact that, the melting point of the crystalline phase of a PAEK material tends to correspond the temperature at which it is formed. This explanation can be corroborated by the observation in [26], where Tardif et. al. reveal that the melting points of PEEK150 are increasing under the increasing crystallisation temperatures. Comparing both materials under the same temperature profile, PAEK1 crystallises quicker than PAEK2, meaning most of its crystalline structures were formed at higher temperatures, leading to higher melting points being detected in remelt. The same principle could be applied to explain the melting point shifts in Fig. 5. As the processing time increased, crystalline structures were formed at lower temperatures, generating endothermic curves with lower characteristic melting points in remelt.

For PAEK1 at $z_0$, an additional endothermic shoulder at around 295 °C appeared with increasing processing time, indicating a possible secondary crystallisation with less perfect crystalline structures. These structures might contribute to the inferior mechanical properties of PAEK1 PBF parts, which is discussed in Section 3.4.

In Fig. 6, the isothermal crystallisation kinetics of PAEK1 and PAEK2 were compared with their in-process crystallisation kinetics. The obvious discrepancy validates again the non-isothermal nature of the PBF process. The trends in Fig. 6 demonstrate that crystallisation at a certain time in one sample will differ depending on the position within the powder bed, which could lead to non-uniform shrinkage and possible distortion of the part. However, the overall in-process

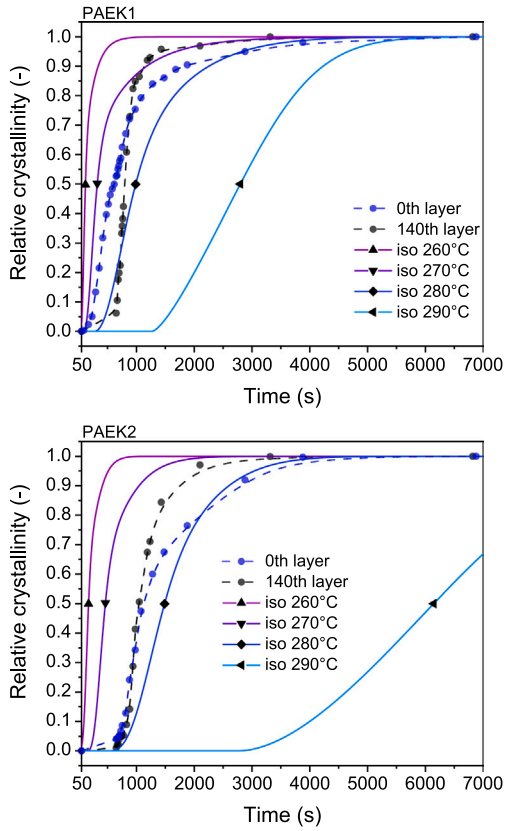


**Fig. 6.** Evolution of crystallisation during printing versus isothermal crystallisation. Dash lines are trends.

**Table 2**
Mechanical properties of printed PAEK tensile bars in comparison with their injection moulded counterparts.

| Process | Material | Modulus (MPa) | XY strength (MPa) | Elongation at break (%) |
|---|---|---|---|---|
| **PBF** | **EOS HP3**[a] | 4250 ± 150 | 90 ± 5 | 2.8 ± 0.2 |
| | **PEEK 450PF**[a] | 5055 ± 690 | 72.0 ± 4.9 | 6.4 ± 1.1 |
| | **PAEK2** | 3207 ± 323 | 83.2 ± 4.4 | 13.6 ± 3.3 |
| | **PAEK1** | 3241 ± 117 | 63.0 ± 3.6 | 4.9 ± 0.4 |
| **IM** | **EOS HP3** [30] | 4300[b] | 97 ± 0.5 | 31.3 ± 1.5 |
| | **PEEK 450**[c] | 4555 ± 209 | 90.6 ± 0.9 | 43.1 ± 3.8 |
| | **PAEK2**[c] | 3646 ± 727 | 81.8 ± 0.8 | 199.7 ± 22.3 |
| | **PAEK1**[c] | 3649 ± 345 | 84.6 ± 1.2 | 27.3 ± 8.0 |

[a] ISO 527–2–1 A type FFF tensile bars were printed using EOS P800 system according to the settings published in [8].

[b] The modulus was taken from the datasheet of HT22 [9], since the injection moulded grade Victrex HT22 is equivalent to the PBF grade PEK HP3 [31].

[c] ISO 527–2–1 A type injection moulded tensile bars were provided by Victrex.

crystallisation behaviour of PAEK2 seems less sensitive to the thickness $z_n$ at the first 1000 s. This could increase the overall stability when printing PAEK2 parts.

In summary, PAEK2 crystallises slower both isothermally and dynamically, owing to the suppressed chain mobility due to less ketone content and more repeating units on the molecular backbone. Specifically, for printing a specimen of 2 mm thickness with PAEK2 powder, most of crystallisation (> 95%) occurs in the cooling phase after the completion of part fabrication.

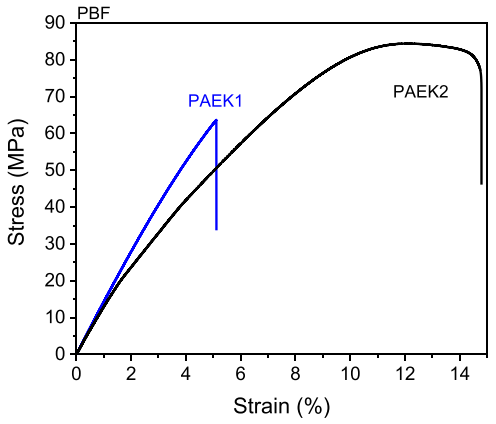


**Fig. 7.** Stress-strain behaviour of the PBF tensile bars.

### 3.4. Mechanical properties

The tensile properties of PBF samples and of their injection moulded counterparts were summarised in Table 2. A set of typical stress-strain curves of PAEK1 and PAEK2 specimens that are close to the mean data are presented in Fig. 7. Compared to the PAEK1 PBF specimens, PAEK2 PBF specimens show a significantly higher mean value of elongation at break by a factor of 2. Fractured PAEK2 PBF specimens displayed signs of plastic yielding, which was never observed on crystalline PBF specimens made of any other PAEK materials.

In general, injection moulded specimens show superior tensile strength and elongation at break than that of PBF specimens. This finding is consistent with the results reported on printing polyamide [27], polypropylene [28], and poly(butylene terephthalate) [29]. Two reasons have been proposed previously [28] to explain the differences in tensile properties. First, the mechanical properties are sensitive to voids. PBF specimens contain voids accelerating crack initiation, leading to inferior toughness and ductility. Second, injection moulded specimens have lower degree of crystallinity, which facilitates ductile deformation. To verify the influence of crystallinity on mechanical properties of PAEK specimens, the overall crystallinities for each type of specimen were calculated from the X-ray diffraction profiles, presented in Fig. 8.

As listed in Fig. 8, for each material, the PBF specimen presents a higher degree of crystallinity than that of the injection moulded counterpart. These results agree with the findings of previous studies on other semi-crystalline polymers [27–29]. Differences in crystallinity could be attributed to the different thermal histories of the two manufacturing processes. In PBF, during melting, the extremely fast temperature surge produced by the laser emission [25] could cause incomplete melting of the powder. The residual ordered segments could trigger self-nucleation [32], contributing to higher degrees of crystallinity in the printed parts. Compared with the PBF process, PAEKs in the injection moulding process often undergo a longer heating stage erasing all the crystalline memory, leading to isotropic melts. Hence, the nucleation densities were reduced, producing parts with lower degrees of crystallinity. During cooling, as clear from the temperature profiles in Fig. 2, PBF specimens went through a slow cooling phase with relatively low cooling rates, allowing more crystal growth. In contrast, injection moulded specimens were likely to experience a rapid cooling phase after ejection [27], leading to lower degrees of crystallinity.

XRD results prove that the high elongation values of the injection moulded PAEK2 specimens are mainly due to a low crystallinity and a high content of amorphous phase. On the other hand, the PBF PAEK1 and the PBF PAEK2 specimens have similar crystallinities. Moreover, the flowability data in the Supplementary Material suggests that the flowability of PAEK2 is inferior to PAEK1, even though PAEK2 printed parts showed superior mechanical properties. Comparing these two, it can be concluded that the high elongation values of PBF PAEK2 specimens are

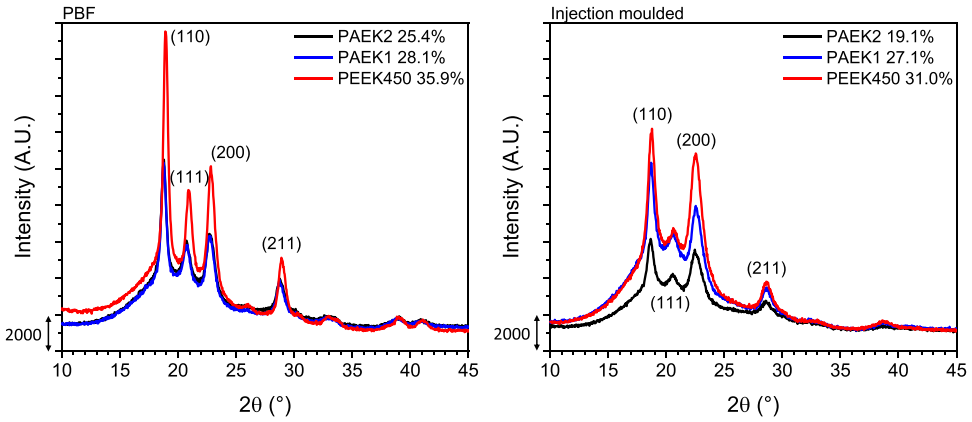


**Fig. 8.** Diffraction profiles for PBF and injection moulded specimens. The corresponding crystallographic planes of four major crystalline peaks were marked out. The degrees of crystallinity were calculated according to Eq. (1).

mainly the result of its slow crystallising nature. The influence of powder properties is far less dominant than the influences of crystallisation kinetics. Slow crystallisation delays the impediment to chain mobility, leading to better particle coalescence and interlayer adhesion. As revealed in Fig. 7, the bonding formed in PBF PAEK2 specimens was sufficient to delocalise the region of the neck, permitting the neck to propagate before failure. The tensile strength of PBF PAEK2 specimens reflects the bulk properties rather than the bonding strength, unlike PBF specimens made of any other PAEK materials. Previously, the improvement on the elongation values of PBF PAEK parts was achieved by shortening the cooling time, but this method only lead to ductile yet amorphous PAEK parts [20]. It should be emphasised that, PAEK2 is the first PAEK grade to achieve high elongation values while maintaining high degrees of crystallinity in the PBF process.

It should be emphasised as well that, although the printed PAEK1 and PAEK2 parts reached similar overall crystallinities, the differences in crystallising path between the two polymeric grades significantly influence the mechanical properties. Similarly, the crystallisation paths within one printed specimen at different powder deposition thicknesses vary. For example, at 2000 s, the crystallinities of a PAEK2 part at $z_0$ and at $z_{140}$ are 19.8% and 23.9%, respectively. The anisotropic crystallisation could potentially cause uneven shrinkage across the part. Hence, in the future, a more interactive (parameter-adapted) machine is desired to achieve the optimal mechanical properties with the minimal part distortion.

## 4. Conclusions

The paper presents a new PAEK family of backbone modified PEEK grades in the application of high temperature PBF process. The insertion of PEDEK comonomer onto the PEEK molecular backbone successfully reduced the powder bed temperature to 290 °C. The lower powder bed temperature is expected to reduce the level of thermo-oxidative degradation and cross-linking, therefore, improve the recyclability of the powder. The specific in-process temperature profiles were constructed and replicated using the flash DSC. This method allowed understanding the crystallisation evolution within the PBF process. Among the new polymers, PAEK2 with a tailored molecular weight has a significantly slower crystallisation kinetics which leads to better particle coalescence in the PBF process. The results revealed that, for PAEK polymers, slow crystallising is beneficial to better mechanical properties such as a higher elongation at break. This finding points out a possible route to developing new polymers for the PBF process that could potentially match their bulk mechanical properties. The results also revealed that, depending on the size of the part (varied $z_n$) within the PBF process, a part can experience different crystallisations at the same time, leading to part distortion and variation in mechanical performance. Therefore, this research may establish a foundation for the future development of a more interactive (parameter-adapted) printing machine to minimise part distortion and to optimise part mechanical properties.

## CRediT authorship contribution statement

**Ghita Oana:** Writing – review & editing, Supervision, Conceptualization. **Davies Richard:** Writing – review & editing, Methodology. **Chaplin Adam:** Writing – review & editing, Resources. **Yi Nan:** Writing – original draft, Software, Methodology, Investigation, Formal analysis.

## Declaration of Competing Interest

The authors declare that they have no known competing financial interests or personal relationships that could have appeared to influence the work reported in this paper.

## Appendix

This appendix elaborates the method to construct the temperature profiles in Fig. 2. All constructed temperature profiles comprised three segments. The first segment describes the cooling of the *n*-th layer during powder deposition, where the cooling trend was generated by the analytical model given as Eq. (A-1):

$$T(z_n,t)=\frac{(T_{chamber}-T_{platform})}{z_n+\frac{h_{layer}}{t_{layer}}t}\quad z_n+T_{platform} \tag{A-1}$$

where $T(z_n,t)$ is the temperature of the *n*-th layer simulated at time *t*; $T_{chamber}$ is the chamber temperature (290 °C in this study); $T_{platform}$ is the building platform temperature (260 °C in this study); $h_{layer}$ is the thickness of a single layer (0.12 mm in this study); $t_{layer}$ is the deposition time of a single layer (35.5 s in this study).

Fig. A-1 illustrates the conception of the model. Based on the temperature settings during printing, the boundary conditions were a constant surface temperature at the powder-platform interface, and a constant surface heat flux at the powder-air interface. Several assumptions were taken to establish the model in Eq. (A-1). On a macroscopic scale, powder was considered as a continuum with homogenised properties, where temperature variations in the XY plane were neglected. Heat transfer was assumed to be one-dimensional conduction only in the vertical Z direction. The thermal conductivity of the powder bed was taken as a constant. The building platform and the chamber were assumed in steady-state conditions, meaning the temperature remained at $T_{chamber} = 260$ °C and $T_{platform} = 290$ °C. The powder bed was considered in transient conditions, where the latent heat was neglected. Solely for the purpose of numerical prediction, the thickness of powder bed was assumed to be linearly increasing regarding the printing time $t$, at a speed of $\frac{h_{layer}}{t_{layer}}$.

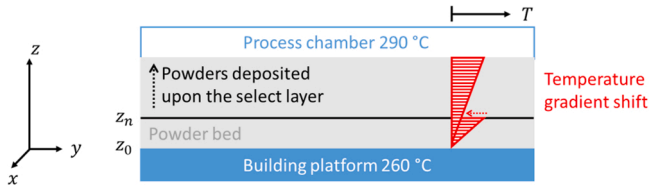


**Fig. A-1.** Modelling of the temperature drop of the $n$-th layer during powder deposition.

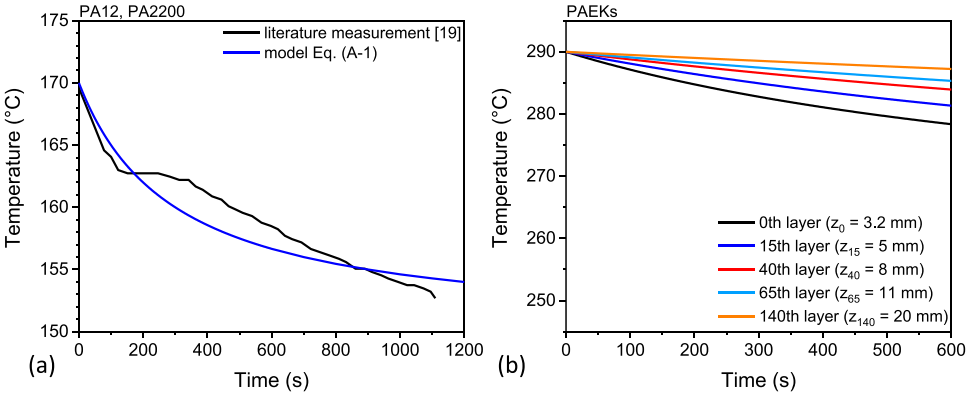


**Fig. A-2.** Verification of modelling and simulated temperature profiles of powder deposition segment.

The proposed analytical model provides a crude estimation of the temperature drop during powder deposition. To verify this model, parameters from the literature on printing polyamides [19] were substituted into Eq. (A-1) to compare with the thermocouple measurements, see Fig. A-2(a). The modelling results were found in reasonably good agreement with the measurements from the literature. The discrepancy in the model and the literature measurements is due to latent heat produced by crystallisation, which could be addressed using a more advanced transient heat transfer model [33]. Nevertheless, Eq. (A-1) successfully estimated the amount of temperature drop during the powder deposition period. Hence, it was proposed in the current work to generate the first segment of the in-process temperature profile, see Fig. A-2(b).

The second segment is the temperature drop during the controlled cooling stage. As displayed in Fig. A-3, profiles of this segment were obtained by monitoring the pyrometer readings at the surface of the powder bed with varied thicknesses under the temperature settings disclosed Section 3.2.1. Besides the two selected thicknesses $z_0$ and $z_{140}$ presented in Section 3.2, powder bed with additional three thicknesses were examined to identify the critical thickness of thermal penetration to be 8 mm. It concludes, when the powder bed is thicker than 8 mm, the impact of the building platform temperature on the powder bed surface temperature is insignificant.

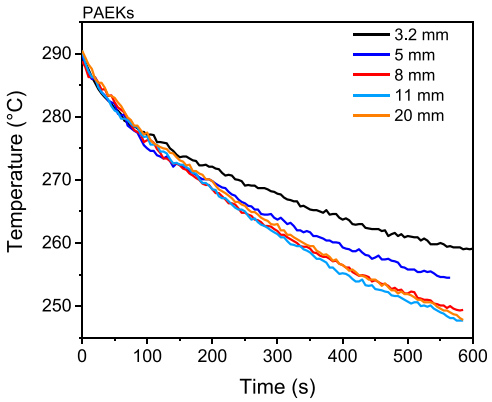


**Fig. A-3.** Measured temperature profiles of the controlled cooling stage.

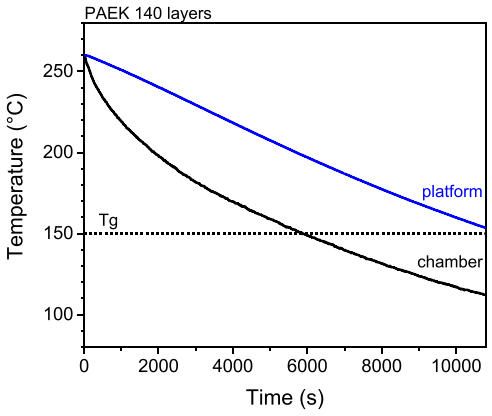


**Fig. A-4.** Measured temperature profiles of the free cooling stage.

The third and the final segment is the temperature drop during the free cooling stage. At $z_0 = 3.2$ mm, the temperature of powder is heavily influenced by the temperature of the building platform. Rapid temperature equalisation between powder at $z_0$ and the building platform is expected. For this reason, the cooling trend of powder at $z_0$ is considered following the same cooling trend of the building platform. In parallel, at $z_{140} = 20$ mm, the temperature of powder is heavily influenced by the temperature of the chamber. Similarly, the cooling trend of powder at $z_{140}$ is considered following the same cooling trend of the chamber. Recordings of the building platform temperature from the thermocouples and the chamber temperature from the pyrometer during the free cooling stage are shown in Fig. A-4.

## Appendix A. Supporting information

Supplementary data associated with this article can be found in the online version at doi:10.1016/j.addma.2022.102857.

## References

[1] C.A. Chatham, T.E. Long, C.B. Williams, Progress in polymer science a review of the process physics and material screening methods for polymer powder bed fusion additive manufacturing, Prog. Polym. Sci. vol. 93 (2019) 68–95, https://doi.org/10.1016/j.progpolymsci.2019.03.003.
[2] A. Das, et al., Current Understanding and Challenges in High Temperature Additive Manufacturing of Engineering Thermoplastic Polymers, in: Additive Manufacturing, Elsevier, 2020, https://doi.org/10.1016/j.addma.2020.101218.
[3] L.J. Tan, W. Zhu, K. Zhou, Recent progress on polymer materials for additive manufacturing, Adv. Funct. Mater. vol. 30 (43) (2020) 1–54, https://doi.org/10.1002/adfm.202003062.
[4] EOS, 2010, P800 Manual, Application notes EOS PEEK HP3 for EOSINT P 800.
[5] O.R. Ghita, E. James, R. Trimble, K.E. Evans, Physico-chemical behaviour of Poly (Ether Ketone) (PEK) in High Temperature Laser Sintering (HT-LS), J. Mater. Process. Technol. vol. 214 (4) (2014) 969–978, https://doi.org/10.1016/j.jmatprotec.2013.11.007.
[6] S. Berretta, K.E. Evans, O.R. Ghita, Predicting processing parameters in high temperature laser sintering (HT-LS) from powder properties, Mater. Des. vol. 105 (2016) 301–314, https://doi.org/10.1016/j.matdes.2016.04.097.
[7] K.C.H. Gardner, B.S. Hsiao, R.R. Matheson, B.A. Wood, Structure, crystallization and morphology of poly (aryl ether ketone ketone), Polym. (Guildf. ) vol. 33 (12) (1992) 2483–2495, https://doi.org/10.1016/0032-3861(92)91128-O.
[8] S. Berretta, K.E. Evans, O. Ghita, Processability of PEEK, a new polymer for high temperature laser sintering (HT-LS), Eur. Polym. J. vol. 68 (2015) 243–266, https://doi.org/10.1016/j.eurpolymj.2015.04.003.
[9] T. Rechtenwald, H.-J. Krauß, D. Pohle, M. Schmidt, Small scale and micro featured functional prototypes generated by laser sintering of polyetheretherketone, Micromach. Technol. Micro-Opt. Nano-Opt. V. Microfabr. Process Technol. XII vol. 6462 (March 2007) (2007), 646203, https://doi.org/10.1117/12.703097.
[10] Victrex PLC, https://www.victrex.com/datasheets, viewed 15 December 2021.
[11] A. Patel, V. Venoor, F.F. Yang, X. Chen, M.J. Sobkowicz, Evaluating poly(ether ether ketone) powder recyclability for selective laser sintering applications, Polym. Degrad. Stab. vol. 185 (2021), https://doi.org/10.1016/j.polymdegradstab.2021.109502.
[12] N. Yi, R. Davies, A. Chaplin, P. McCutchion, O. Ghita, Slow and fast crystallising poly aryl ether ketones (PAEKs) in 3D printing: Crystallisation kinetics, morphology, and mechanical properties, Addit. Manuf. vol. 39 (June 2020) (2021), 101843, https://doi.org/10.1016/j.addma.2021.101843.
[13] D.J. Blundell, V. Bayon, The crystal structure of poly(ether ketone) copolymers, Polym. (Guildf. ). vol. 34 (7) (. 1993) 1354–1360, https://doi.org/10.1016/0032-3861(93)90845-2.
[14] D. Drummer, D. Rietzel, F. Kühnlein, Development of a characterization approach for the sintering behavior of new thermoplastics for selective laser sintering, Phys. Procedia vol. 5 (PART 2) (2010) 533–542, https://doi.org/10.1016/j.phpro.2010.08.081.
[15] A. Amado, K. Wegener, M. Schmid, G. Levy, Characterization and modeling of non-isothermal crystallization of Polyamide 12 and co-Polypropylene during the SLS process, 5th Int. Polym. Mould. Innov. Conf. (2012) 60.
[16] F. Neugebauer, V. Ploshikhin, J. Ambrosy, G. Witt, Isothermal and non-isothermal crystallization kinetics of polyamide 12 used in laser sintering, J. Therm. Anal. Calorim. vol. 124 (2) (2016) 925–933, https://doi.org/10.1007/s10973-015-5214-8.
[17] P. Chen, et al., Crystallization kinetics of polyetheretherketone during high temperature-selective laser sintering, Addit. Manuf. vol. 36 (May) (2020), https://doi.org/10.1016/j.addma.2020.101615.
[18] L.J. Tan, W. Zhu, K. Sagar, K. Zhou, Comparative study on the selective laser sintering of polypropylene homopolymer and copolymer: processability, crystallization kinetics, crystal phases and mechanical properties, Addit. Manuf. vol. 37 (April 2020) (2021), https://doi.org/10.1016/j.addma.2020.101610.
[19] D. Drummer, S. Greiner, M. Zhao, K. Wudy, A novel approach for understanding laser sintering of polymers, in: Addit. Manuf, vol. 27, 2019, pp. 379–388, https://doi.org/10.1016/j.addma.2019.03.012.
[20] L. Benedetti, B. Brulé, N. Decraemer, R. Davies, K.E. Evans, O. Ghita, A route to improving elongation of high-temperature laser sintered PEKK, Addit. Manuf. (July) (2020), 101540, https://doi.org/10.1016/j.addma.2020.101540.
[21] D. Hansen, R.C. Kantayya, C.C. Ho, Thermal conductivity of high polymers - the influence of molecular weight, Polym. Eng. Sci. vol. 6 (3) (. 1966) 260–262, https://doi.org/10.1002/pen.760060315.
[22] J. Seo, et al., Isothermal crystallization of poly(ether ether ketone) with different molecular weights over a wide temperature range, Polym. Cryst. vol. 2 (1) (2019), https://doi.org/10.1002/pcr2.10055.
[23] M. Yuan, J.A. Galloway, R.J. Hoffman, S. Bhatt, Influence of molecular weight on rheological, thermal, and mechanical properties of PEEK, Polym. Eng. Sci. vol. 51 (1) (. 2011) 94–102, https://doi.org/10.1002/pen.21785.
[24] S. Josupeit, L. Ordia, H.J. Schmid, Modelling of temperatures and heat flow within laser sintered part cakes, Addit. Manuf. vol. 12 (2016) 189–196, https://doi.org/10.1016/j.addma.2016.06.002.
[25] P. Peyre, Y. Rouchausse, D. Defauchy, G. Régnier, Experimental and numerical analysis of the selective laser sintering (SLS) of PA12 and PEKK semi-crystalline polymers, J. Mater. Process. Technol. vol. 225 (2015) 326–336, https://doi.org/10.1016/j.jmatprotec.2015.04.030.
[26] X. Tardif, et al., Experimental study of crystallization of PolyEtherEtherKetone (PEEK) over a large temperature range using a nano-calorimeter, Polym. Test. vol. 36 (2014) 10–19, https://doi.org/10.1016/j.polymertesting.2014.03.013.
[27] B. Van Hooreweder, D. Moens, R. Boonen, J.-P. Kruth, P. Sas, On the difference in material structure and fatigue properties of nylon specimens produced by injection molding and selective laser sintering, Polym. Test. vol. 32 (5) (. 2013) 972–981, https://doi.org/10.1016/j.polymertesting.2013.04.014.
[28] W. Zhu, C. Yan, Y. Shi, S. Wen, J. Liu, Y. Shi, Investigation into mechanical and microstructural properties of polypropylene manufactured by selective laser sintering in comparison with injection molding counterparts, Mater. Des. vol. 82 (. 2015) 37–45, https://doi.org/10.1016/j.matdes.2015.05.043.

[29] S. Arai, S. Tsunoda, R. Kawamura, K. Kuboyama, T. Ougizawa, Comparison of crystallization characteristics and mechanical properties of poly(butylene terephthalate) processed by laser sintering and injection molding, Mater. Des. vol. 113 (2017) 214–222, https://doi.org/10.1016/j.matdes.2016.10.028.

[30] O. Ghita, et al., High Temperature Laser Sintering (HT-LS): an investigation into mechanical properties and shrinkage characteristics of Poly (Ether Ketone) (PEK) structures, Mater. Des. vol. 61 (2014) 124–132, https://doi.org/10.1016/j.matdes.2014.04.035.

[31] S. Berretta, Y. Wang, R. Davies, O.R. Ghita, Polymer viscosity, particle coalescence and mechanical performance in high-temperature laser sintering, J. Mater. Sci. vol. 51 (10) (2016) 4778–4794, https://doi.org/10.1007/s10853-016-9761-6.

[32] A.J. Müller, R.M. Michell, R.A. Pérez, A.T. Lorenzo, Successive self-nucleation and annealing (SSA): correct design of thermal protocol and applications, Eur. Polym. J. vol. 65 (2015) 132–154, https://doi.org/10.1016/j.eurpolymj.2015.01.015.

[33] F. Shen, W. Zhu, K. Zhou, L. Ke, Modeling the temperature, crystallization, and residual stress for selective laser sintering of polymeric powder, Acta Mech. (. 2021), https://doi.org/10.1007/s00707-021-03020-6.